Environmental Health Engineering and Management Journal 2022, 9(3), 311-318
http://ehemj.com
doi 10.34172/EHEM.2022.32

Environmental Health Engineering and Management Journal

Original Article

Environmental Health Engineering and Management

Open Access Publish Free

Photocatalytic removal of ciprofloxacin antibiotic from aqueous medium by applying AgI/Ag_2O nanocomposite: Activity test, reaction kinetics, and catalyst reusability

Mehdi Ahmadmoazzam[1,2], Afshin Takdastan[1,2*], Abdolkazem Neisi[1,2], Mehdi Ahmadi[1,2], Ali Babaei[1,2], Sahand Jorfi[1,2]

[1]Department of Environmental Health Engineering, Ahvaz Jundishapur University of Medical Sciences, Ahvaz, Iran
[2]Environmental Technologies Research Center, Ahvaz Jundishapur University of Medical Sciences, Ahvaz, Iran

Abstract

Background: This study examined the removal of ciprofloxacin (CIP), which is a very widely used antibiotic, from an aqueous medium by applying AgI/Ag_2O photocatalyst under visible light radiation.

Methods: AgI/Ag_2O was synthesized conveniently by applying a two-stage precipitation method. The synthesized compound was characterized by X-ray powder diffraction (XRD), FE- field emission scanning electron microscopy (FE-SEM), energy dispersive x-ray (EDX), and UV-Vis spectrophotometry. Different parameters including initial pH of the solution, initial CIP concentration, reaction kinetics, and catalyst reusability were investigated.

Results: Concurrent use of AgI and Ag_2O caused improved photocatalytic properties in the presence of UV light. The pH and initial concentration of CIP affected the process efficiency; 95% efficiency was achieved within 100 min at pH 9. Furthermore, the process efficiency was still maintained over 90% after four consecutive cycles.

Conclusion: The photocatalytic degradation process using AgI/Ag_2O nanocomposite under visible light radiation is a suitable method for removing CIP from aqueous media due to its high efficiency and stability.

Keywords: Ciprofloxacin, Nanocomposites, Photolysis, Catalysis, Antibiotic, Aqueous medium

Citation: Ahmadmoazzam M, Takdastan A, Neisi A, Ahmadi M, Babaei A, Jorfi S. Photocatalytic removal of ciprofloxacin antibiotic from aqueous medium by applying AgI/Ag2O nanocomposite: Activity test, reaction kinetics, and catalyst reusability. Environmental Health Engineering and Management Journal 2022; 9(3): 311-318. doi: 10.34172/EHEM.2022.32.

Article History:
Received: 7 January 2022
Accepted: 2 March 2022
ePublished: 10 September 2022

***Correspondence to:**
Afshin Takdastan,
Email: afshin_ir@yahoo.com

Introduction

Today antibiotics are widely used in the treatment of human and animal bacterial infections. However, once the residuals of these compounds leave the body, they enter the environment and threaten the health of the system (1). Ciprofloxacin (CIP) is an antibiotic belonging to the second-generation fluoroquinolones, which can treat different bacterial infections (2,3). The entrance of this substance into the nature can cause bacterial drug resistance. Recently, studies have reported the presence of CIP residuals in aqueous resources and effluent of wastewater treatment plants (4,5). Unfortunately, the conventional methods cannot remove CIP completely, therefore, newer methods should be investigated (6). Advanced oxidation processes (AOPs) have recently been introduced as a promising option for the removal of CIP from aqueous media (7). AOPs are the processes based on the production of highly oxidizing radical species that react with organic matter, and eventually, lead to their degradation (8).

One of these methods is photocatalytic processes using semiconductor materials, which have shown a high ability in degrading organic contaminants (9,10). The electronic structure of most semiconductor materials consists of a band with the highest electron content called the valence band and an unoccupied band called the conduction band (11,12). These bands are separated by an area that largely lacks energy levels, which is called the band gap. The irradiation of these materials with more energy than their band gap produces a hole electron pair (h^+ e^-), which can be possible to react with adsorbed species (7,13). These processes possess features including being economical as well as operability at ambient temperature and pressure (14-16). Nevertheless, photocatalytic processes are still under study and enhancement. However, various compounds have attracted attention to be used as new photocatalysts (17,18). In different studies, various semiconductors have been explored, mostly introducing

silver-based compounds as stable, economical, and highly efficient semiconductors (19,20). Among Ag-based semiconductors, Ag_2O (1.2 eV) and AgI (2.26 eV) with their appropriate bandgap are very suitable in the presence of visible light (21,22). Nevertheless, to find a suitable semiconductor with all economic and technical features, further studies are required so that all parameters affecting the photocatalytic removal process could be examined and compared.

Although studies have been performed on examining the efficiency of photocatalysts for antibiotic removal, most of them have been undertaken based on the UV light, and there are sparse studies on the effect of visible light on the efficiency of these processes (23). LED lights can be a suitable alternative to mercury vapor and xenon lamps in this type of process because of their desirable features such as long-life span, low energy consumption, low toxicity, and being environmentally friendly.

Thus, to explore some of the mentioned issues, in this study, AgI/Ag_2O photocatalyst was synthesized conveniently by applying a two-stage precipitation method, and then, utilized for CIP removal. Furthermore, the physiochemical properties of the synthesized catalyst were investigated plus the effect of important parameters on the process efficiency and the catalyst stability in four consecutive cycles.

Materials and Methods

Catalyst preparation

AgI/Ag_2O was synthesized with an equal mole ratio of 1:1 by a simple two-stage precipitation method at room temperature. Initially, 1.66 g of KI and 1.7 g of $AgNO_3$ were separately added to 50 mL of distilled water and stirred at room temperature. Next, $AgNO_3$ solution was added dropwise to the KI solution while being stirred; after 30 minutes of mixing, a yellow suspension was formed, which was separated from the solution through centrifugation, washed several times with distilled water, and eventually, dried in an oven at 50°C for 12 hours. The AgI of the previous stage was dispersed in 20 mL distilled water and stirred for 30 minutes. Subsequently, 1.7 g of $AgNO_3$ dissolved in 50 mL of distilled water was added dropwise to the above-mentioned suspension and stirred at room temperature for 30 minutes. Next, 100 mL of NaOH 1 M solution was added immediately to the previously prepared solution and stirred again for 30 minutes. Eventually, the obtained suspension was separated through centrifugation, and after several times of washing with distilled water at 50°C, it was dried in the oven for 12 hours (24,25).

Catalyst characteristics

X-ray powder diffraction (XRD) test was performed to investigate the structure of the crystalline phase of the synthesized samples using an X-ray diffraction device (D8 Bruker) and CuKα radiation at the wavelength of 1.54 Å, voltage 40 kV, current 40 mA, and 2θ angle between 10 and 80°. Ultraviolet radiation spectrum measurement was performed to specify the optical properties of the synthesized samples within 200-800 nm using a UV-Vis device (Thermo Co., USA) to characterize the optical properties of the synthesized samples. The morphological features and structure of the synthesized catalyst were investigated by field emission scanning electron microscopy (FE-SEM) equipped with an energy dispersive x-ray (EDX) spectrometry device (TESCAN Co., Model III MIRA) to investigate the composition of the elements present in the synthesized catalyst.

Photocatalytic activity test

The photocatalytic activity of the synthesized catalyst was measured by degrading a solution containing specific concentration of CIP under visible light radiation. For this purpose, a 500-mL quartz container containing 200 mL CIP solution was used with a concentration of 1 mg/L, 0.2 g AgI/Ag_2O, and a 100-W LED lamp. Before initiating the photocatalytic process, to achieve the absorption and desorption equilibrium of CIP on the catalyst surface, stirring was performed for 30 minutes in darkness, after which the light was turned on. Here, 2 mL was withdrawn from the solution at specific time intervals, and after centrifugation at 6000 rpm and passage through a head syringe, 0.2 micron was injected into the high-performance liquid chromatography (HPLC) device to determine CIP concentration. The removal efficiency was determined by Eq. (1).

$$CIP\ removal\,(\%) = \frac{CIP_0 - CIP_t}{CIP_0} \times 100 \quad (1)$$

Analytical methods

CIP concentration was measured using HPLC device (KNAUER, Germany) equipped with C18 (5-100) column and UV detector at a wavelength of 278 nm. Mobile phase containing water and acetonitrile (75 to 25 v/v ratio) containing 0.3% formic acid and a flow rate of 1 mL/min was used. The peak time wavelength of CIP was between 1.6 and 1.7 minutes, with the measurement continuing up to 10 minutes. To draw a standard curve, 0.1-50 mL/L concentrations of CIP were used. The R-squared (R^2) for the obtained standard curve was 0.99. The limit of detection (LOD) and the limit of quantification (LOQ) for CIP were 0.05 and 0.2 mg/L, respectively.

Pseudo-first order kinetic equations were used to determine the degradation reaction constant and CIP half-life (according to reaction (2)):

$$L_n \frac{c_0}{c_t} = k_t \quad (2)$$

Where k represents the reaction constant (min^{-1}), t denotes the reaction time (min), C_0 shows the initial CIP concentration (mg/L), and C_t indicates the CIP concentration at time t.

Results

Catalyst features

XRD analysis was performed to investigate the structure of the crystalline phase of the synthesized samples. Figure 1a indicates the XRD pattern associated with AgI and Ag_2O alongside AgI/Ag_2O composite. UV-Vis DRS method was applied to specify the optical properties of the synthesized samples; the results are shown in Figure 1b. The morphological features of the synthesized samples were characterized through FE-SEM images. Figure 2a indicates the images related to AgI/Ag_2O. In addition, EDX analysis was also performed to investigate the composition of elements present in AgI/Ag_2O (Figure 2b).

Assessing the efficiency of the photocatalytic process

The photocatalytic efficiency of Ag_2O, AgI, and AgI/Ag_2O was investigated by measuring the extent of removal of CIP under visible light radiation (Figure 3). The direct CIP photolysis test (control) indicated that CIP concentration did not change compared to the initial concentration. With regards to AgI, Ag_2O, and AgI/Ag_2O, the CIP removal efficiency after 100 min of reaction time was observed 45, 58, and 95%, respectively.

The effect of operational parameters on the CIP photocatalytic removal

The effect of CIP initial concentration

To explore the effect of initial CIP concentration on the photocatalytic removal efficiency, experiments were performed with three different concentrations including 1, 5, and 30 mg/L. As seen in Figure 4a, the elevation of the CIP initial concentration led to a considerable reduction of removal efficiency; after 100 minutes of reaction time, the removal efficiency was obtained 95%, 76%, and 44%

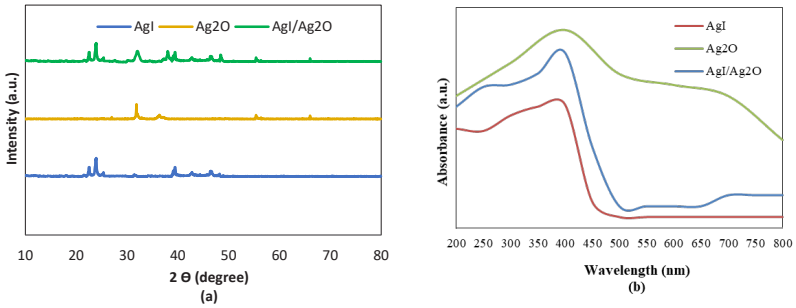

Figure 1. XRD pattern (a) and UV-VIS spectra (b) of the synthesized material.

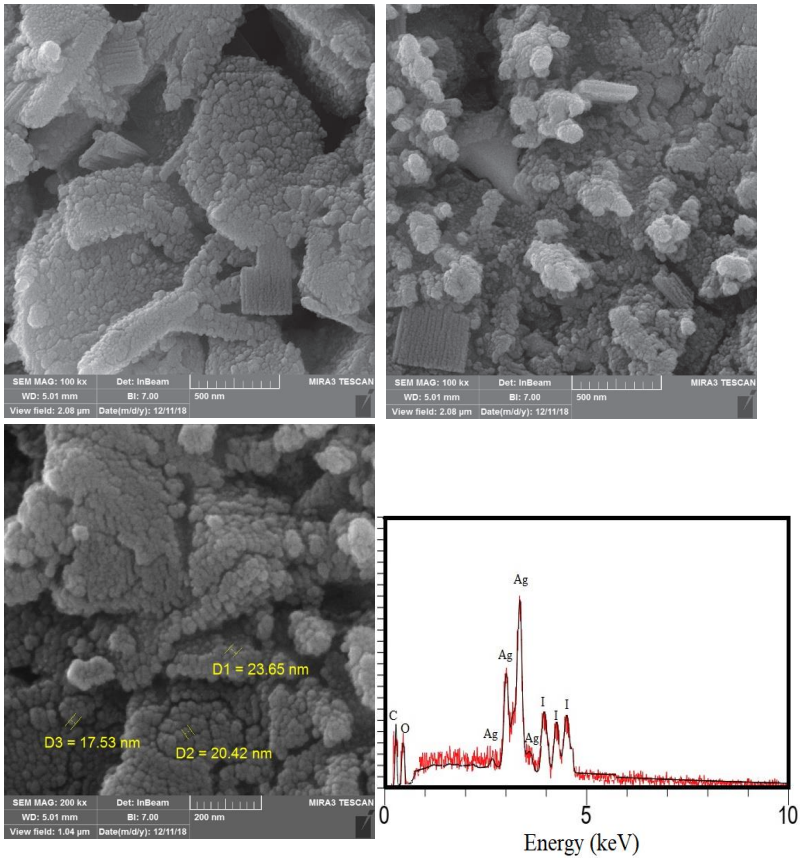

Figure 2. FE-SEM image (a) and EDX spectrum (b) of the synthesized AgI/Ag_2O.

for initial concentrations 1, 5, and 30 mg/L, respectively. Also, to investigate the CIP removal reaction constant at different concentrations, the first-order kinetics was investigated through the linear drawing of ln C/C_0 against radiation time (t), where the line slope indicated the reaction rate constant (Figure 4b). The high correlation coefficient of the photocatalytic removal reaction (R^2>0.98) for different concentrations of CIP indicates that the reaction rate could be described by the pseudo-first-order kinetic model.

Effect of initial pH

The impact of different initial pH on CIP for the catalytic removal process was examined at pH levels of 2.5-11. The results showed that CIP removal was associated with changes in the initial pH of the solution. The results indicated that the removal efficiency was higher at alkaline pH than at acidic pH; the largest efficiency (95%) was obtained at pH 9 (Figure 5a). Furthermore, after calculation, the point of pH at which the superficial charges of the catalyst are zero (pHpzc) was obtained 10. This suggests that the catalyst surface at pH values above 10 was negatively charged, and at values below 10 was positively charged.

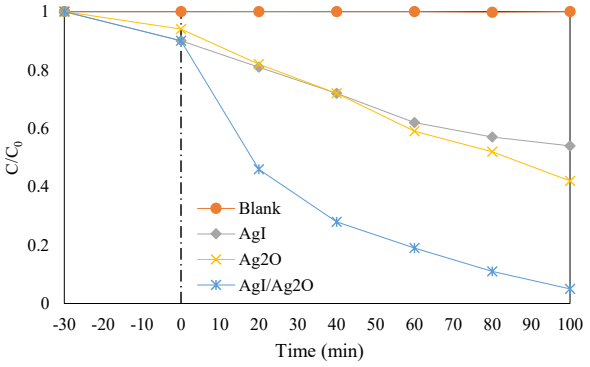

Figure 3. CIP degradation under visible light with various photocatalysts.

Measurement of the catalyst stability during four consecutive cycles

To explore the stability of the synthesized catalyst, the CIP removal process was measured during four consecutive cycles of reaction (Figure 5b). As seen, despite the reduction of process efficiency after four consecutive cycles, the process has still maintained more than 90% of its efficiency compared to the initial state.

Effect of scavengers

To identify the photocatalytic removal reaction mechanism of CIP by AgI/Ag_2O, the main oxidative species active in the photocatalytic process were determined by scavenging test using triethanolamine (TEOA, as h^+ scavenger), tert-Butyl alcohol (tert-BuOH, as $OH^•$ Scavenger), and benzoquinone (BQ, as $O2^{-•}$ scavenger). The results are shown in Figure 6a.

CIP mineralization capability

CIP mineralization capability was investigated during

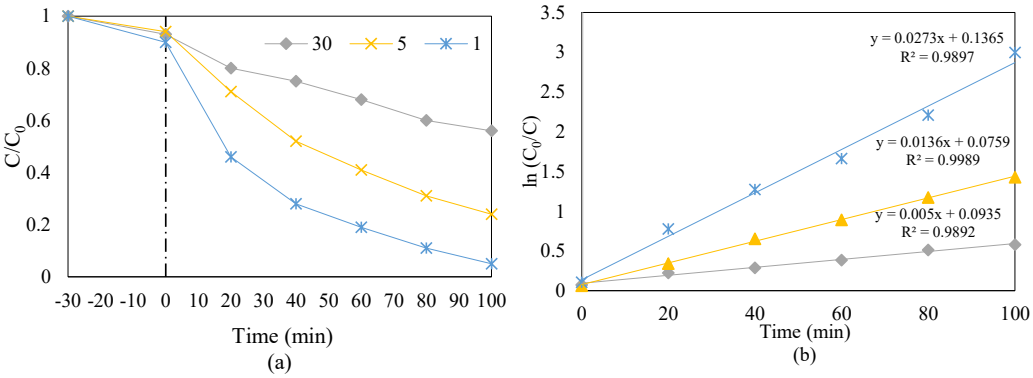

Figure 4. Effect of initial CIP concentration (a) and kinetic curves of initial CIP concentration (b) over photocatalytic process.

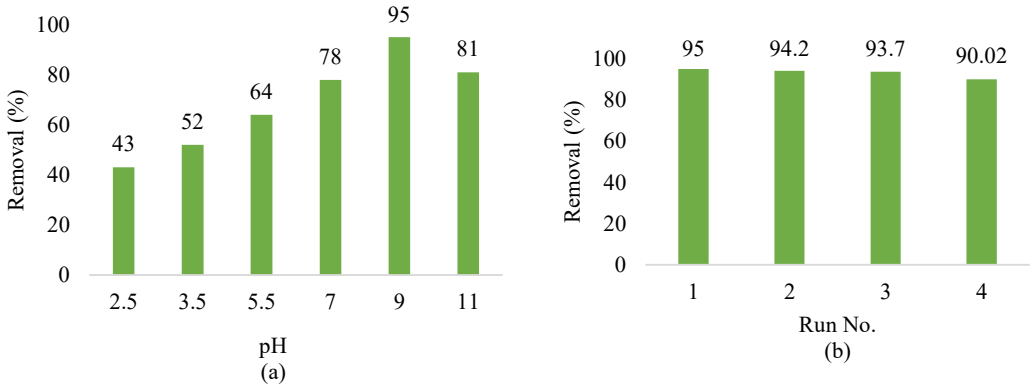

Figure 5. Effect of initial pH on CIP removal (a) and the reusability test of AgI/Ag_2O.

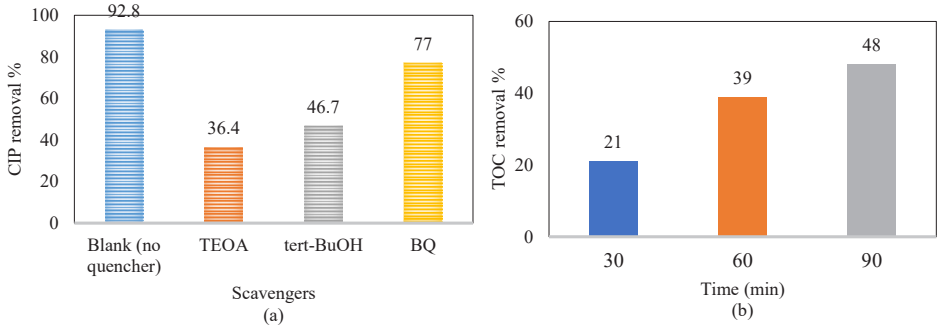

Figure 6. Effect of different radical scavengers on the CIP removal efficiency by AgI/Ag_2O (a) and TOC removal efficiency (b).

different reaction times by measuring the removal efficiency of TOC (Figure 6b).

CIP removal from real wastewater medium

A real wastewater matrix (the output of a secondary treatment unit) spiked with CIP (1 mg/L) was used to investigate the effect of the real wastewater matrix on the process efficiency. Table 1 represents the properties of the real wastewater matrix. As seen, the real wastewater matrix contains some amounts of organic materials and anions, which can affect the process efficiency. According to the results, the obtained removal efficiency of CIP in an aqueous medium decreased from 95% to 54% in the real wastewater matrix.

Discussion

The properties of the synthesized samples were characterized through XRD, UV-Vis DRS, FE-SEM, and EDX methods. The observed peaks associated with AgI (including (100), (002), (101), (102), (110), (103), and (112)) indicate the formation of the hexagonal β-AgI phase (according to JCPDS card No. 09-0374) (26, 27). The peaks associated with Ag_2O (including (110), (111), (200), (220), and (311)) at 2θ angles of 26.8°, 2.33°, 2.38°, 4.55°, and 65.7° reveal the formation of the Ag_2O cubic crystalline phase (according to the JCPDS Card No. 41-1104) (28). The XRD pattern related to the AgI/Ag_2O composite includes the phases associated with AgI and Ag_2O concurrently, suggesting the simultaneous presence of both compounds in the synthesized sample. According to the results obtained from the UV-VIS test, AgI shows an absorption edge at the wavelength of 460 nm corresponding to the bandgap at 2.69 eV. Considering Ag_2O, suitable light absorption within a wide wavelength of 200 to 800 nm can be observed, suggesting light absorptivity within both UV and visible light range as well as its high photocatalytic activity (29,30). Regarding the AgI/Ag_2O composite, the intensity of visible light absorption has grown by adding Ag_2O to AgI. The wavelength thresholds of the composites were calculated to be 520 nm corresponding to the bandgap at 2.38 eV. This suggests that the AgI/Ag_2O composite enhanced light absorptivity compared to pure AgI and increased the utilization efficiency of visible light. Investigation of FE-SEM images shows the formation of all three particles as pseudo-spherical particles with a size smaller than 30 nm; the AgI particles have been formed with a mean size of 12.98 nm and Ag_2O particles with a mean size of 20.53 nm. Also, according to the EDX results, the peaks related to the constituent elements of the composite including Ag, I, and O were detected, well confirming that the composite contains the elements associated with the utilized compounds. The AgI/Ag_2O is composed of Ag, I, and O elements with percentages of 63.2%, 21.4%, and 13.8%, respectively.

Table 1. Characteristics of the real wastewater matrix

Parameter	Concentration	Unit
COD	57.4	Mg L^{-1}
BOD_5	23.8	Mg L^{-1}
TOC	8.94	Mg L^{-1}
TSS	23.7	Mg L^{-1}
TDS	365	Mg L^{-1}
pH	8.1	-
Turbidity	6.2	NTU
Nitrate	1.72	Mg L^{-1}
Sulfate	28.9	Mg L^{-1}
Chloride	35.3	Mg L^{-1}
Bicarbonate	158	Mg L^{-1}

The results of examining the CIP photocatalytic removal efficiency by Ag_2O, AgI alone, as well as the concurrent presence of these compounds as AgI/Ag_2O composite confirm that the photocatalytic activity of the synthesized composite has grown considerably compared to that of pure Ag_2O and AgI. Indeed, modification of AgI with Ag_2O has improved its photocatalytic properties in the presence of visible light; CIP has been removed by 95% within 100 minutes.

The results of exploring the effect of the initial concentration of CIP on the process efficiency showed that CIP degradation at lower concentrations has occurred more rapidly, and with an increase in the initial concentration, the time required for its degradation has also been prolonged. Specifically, for 1 mg/L concentration, 95% degradation was seen after 100 minutes of reaction, while for 5 and 30 mg/L concentrations, the removal efficiency was obtained 76 and 44% within a similar time. Indeed,

the active species affecting the reaction are constant, while more molecules of CIP exist in the solution with the elevation of its concentration. Furthermore, at higher CIP concentrations, larger values of the energy irradiated to the solution are absorbed by CIP molecules. Thus, with the reduction of the energy received by the catalyst surface, its photocatalytic activity diminishes (31,32). The rate constant values (min^{-1}) for concentrations of 1, 5, and 30 mg/L were obtained 0.027, 0.014, and 0.005, respectively, suggesting that the reaction rate constant was far larger for 1 mg/L concentration compared to for 30 mg/L concentration. This well indicates the effect of initial concentration on the reaction rate. Similar results with regards to the reduction of reaction constant with the elevation of initial concentration have been reported in many studies (33,34).

The effect of different initial pH of the solution as an important parameter was examined on the CIP photocatalytic removal. The results indicated that CIP removal was associated with changes in the initial pH of the solution. Since CIP has pKa_1 of 6.09 and pKa_2 of 8.74, at pH lower than pKa_1, it is positively charged, at pH above pKa_2, it is negatively charged, and at pH between pKa_1 and pKa_2, it has an equilibrium of positive and negative charges, known as zwitterionic form (35,36). Thus, at pH 9, since the catalyst superficial charge is positive and the CIP superficial charge is negative, the attraction force between the catalyst and CIP is maximum, causing greater absorption of CIP onto the catalyst surface, thereby, boosting the efficiency. On the other hand, at a pH above 10, the surface of both the catalyst and CIP is negatively charged, therefore, efficiency has diminished in this state (37,38).

The reusability of AgI/Ag_2O was examined after four reuse cycles. After completion of each cycle, the catalyst present in the solution was separated from the solution through centrifugation, washed with distilled water three times, and utilized again for the next cycle. The results showed that after the fourth cycle, the efficiency decreased, though despite this reduction, the process was still more than 90% efficient. This suggests the high stability and reusability of the synthesized catalyst. One of the most important reasons behind the reduction of efficiency over different process cycles is the decline in the absorption surfaces of the catalyst because of contamination with CIP or the intermediate products that are produced during its degradation process (39,40). Eventually, the extent of Ag leakage was reported based on the average value measured within four reuse cycles. On average, 3.11 ± 1.2 µg/L silver leaked off the reactor within four reuse cycles.

The main active oxidative species in the photocatalytic process were identified through radical scavenging experiments. In the presence of tert-butyl alcohol and triethanolamine, the CIP removal efficiency decreased by 46.1% and 56.4%, respectively, compared to the control (no scavengers), which indicates the participation of both hydroxyl radicals and hole in the decomposition of CIP. Therefore, the hydroxyl radicals and hole as the main active species produced by the catalyst have played a significant role in the degradation of CIP. The CIP removal efficiency in the presence of benzoquinone decreased to a much lesser extent than the other two mentioned scavengers, and the reduction in efficiency of only 15.8% in its presence indicates that superoxide radicals are not effectively produced by the catalyst during the photocatalytic process. In some similar studies, holes formed in the catalyst capacity band and produced hydroxyl radicals have been identified as the most important active species in the process, although their effect on the process efficiency has been reported differently (41,42).

The mineralization capability of the CIP by AgI/Ag_2O was investigated using TOC removal efficiency. As represented in Figure 6b, TOC removal was raised to 48% by rising photodegradation time, indicating the efficient mineralization capability of the synthesized photocatalyst. Moreover, the result also showed that the CIP mineralization has increased with increasing reaction time, but more reaction time is required for complete mineralization.

The removal efficiency of CIP in the real wastewater matrix was obtained as 54% in the optimum condition, indicating 41% reduction compared to the aqueous medium. This is due to the compounds present in the real wastewater medium, which compete with CIP molecules in reaction with the active species generated by the catalyst, thereby, lowering the efficiency (43).

Conclusion

AgI/Ag_2O composite was synthesized conveniently by applying a two-stage precipitation method at room temperature. The CIP removal efficiency was higher using AgI/Ag_2O than by applying each of the components embedded in the composite alone. Indeed, modification of AgI with Ag_2O could improve its photocatalytic properties in the presence of visible light. The CIP initial concentration and pH affected the process efficiency; the highest removal efficiency was obtained at pH 9, as much as 95%, at CIP concentration of 1 mg/L after 100 min. Maintaining high efficiency to more than 90% after applying the catalyst during four consecutive cycles suggests high efficiency and reusability of the synthesized catalyst during the CIP photocatalytic removal process.

Acknowledgments

This work is a part of the Ph.D. thesis of Mehdi Ahmadmoazzam, Ahvaz Jundishapur University of Medical Sciences (AJUMS), which was financially supported by AJUMS (ETRC-9704).

Ethical issues

The authors certify that all data collected during the study

are as stated in the manuscript, and no data from the study has been or will be published elsewhere separately (Ethical code: IR.AJUMS.REC.1397.297).

Competing interests

The authors declare that they have no conflict of interests.

Authors' contributions

Conceptualization: MAM, Methodology:MAM, Validation:AT, AN, MA, AB and SJ, Investigation:MAM, Resources:MAM, Writing—Original Draft Preparation:MAM, Writing—Review and Editing: AT, AN, Ahmadi, AB and SJ, Visualization:MA, Supervision:AT, AN, MA, AB and SJ, Project Administration:AT, Funding Acquisition: AT

References

1. Mann A, Nehra K, Rana JS, Dahiya T. Antibiotic resistance in agriculture: Perspectives on upcoming strategies to overcome upsurge in resistance. Curr Res Microb Sci. 2021;2:100030. doi: 10.1016/j.crmicr.2021.
2. Fang H, Oberoi AS, He Z, Khanal SK, Lu H. Ciprofloxacin-degrading paraclostridium sp. Isolated from sulfate-reducing bacteria-enriched sludge: Optimization and mechanism. Water Res. 2021;191:116808. doi: 10.1016/j.watres.2021.
3. Kaur Sodhi K, Kumar Singh D. Insight into the fluoroquinolone resistance, sources, ecotoxicity, and degradation with special emphasis on ciprofloxacin. J Water Process Eng. 2021;43: 102218. doi: 10.1016/j.jwpe.2021.
4. Firouzeh N, Malakootian M, Asadzadeh SN, Khatami M, Makarem Z. Degradation of ciprofloxacin using ultrasound/ZnO/oxone process from aqueous solution-lab-scale analysis and optimization. BioNanoScience. 2021;11(2):306-13. doi: 10.1007/s12668-021-00838-1.
5. Tamaddon F, Nasiri A, Yazdanpanah G. Photocatalytic degradation of ciprofloxacin using $CuFe_2O_4$@ methyl cellulose based magnetic nanobiocomposite. MethodsX. 2020;7:100764. doi: 10.1016/j.mex.2019.12.005.
6. Gupta B, Kumar Gupta A, Sekhar Tiwary C, Ghosal PS. A multivariate modeling and experimental realization of photocatalytic system of engineered S–C3N4/ZnO hybrid for ciprofloxacin removal: Influencing factors and degradation pathways. Environ Res. 2021;196:110390. doi: 10.1016/j.envres.2020.
7. Malakootian M, Nasiri A, Asadipour A, Kargar E. Facile and green synthesis of $ZnFe_2O_4$@ CMC as a new magnetic nanophotocatalyst for ciprofloxacin degradation from aqueous media. Process Saf Environ Prot. 2019;129:138-51. doi: 10.1016/j.psep.2019.06.022.
8. Nasiri A, Tamaddon F, Mosslemin MH, Amiri Gharaghani M, Asadipour A. Magnetic nano-biocomposite $CuFe_2O_4$@ methylcellulose (MC) prepared as a new nano-photocatalyst for degradation of ciprofloxacin from aqueous solution. Environmental Health Engineering and Management Journal. 2019;6(1):41-51. doi: 10.15171/EHEM.2019.05.
9. Hasanzadeh M, Jorfi S, Ahmadi M, Jaafarzadeh N. Hybrid Sono-photocatalytic degradation of acid brown 14 using Persulphate and ZnO Nanoparticles: Feasibility and kinetic Study. Int J Environ Anal Chem. 2020;1-14. doi: 10.1080/03067319.2020.1790543.
10. Malakootian M, Nasiri A, Amiri Gharaghani M. Photocatalytic degradation of ciprofloxacin antibiotic by TiO_2 nanoparticles immobilized on a glass plate. Chem Eng Commun. 2020;207(1):56-72. doi: 10.1080/00986445.2019.1573168.
11. Ebrahimi A, Jafari N, Ebrahimpour K, Nikoonahad A, Mohammadi A, Fanaei F, et al. The performance of TiO2/NaY-zeolite nanocomposite in photocatalytic degradation of microcystin-LR from aqueous solutions: Optimization by response surface methodology (RSM). Environmental Health Engineering and Management Journal. 2020;7(4):245-56. doi: 10.34172/EHEM.2020.29.
12. Rangkooy HA, Jahani F, Siahi Ahangar A. Photocatalytic removal of xylene as a pollutant in the air using ZnO-activated carbon, TiO2-activated carbon, and TiO2/ZnOactivated carbon nanocomposites. Environmental Health Engineering and Management Journal. 2020;7(1):41-7. doi: 10.34172/EHEM.2020.06.
13. Amiri Hosseini S, Hashempour Y. Photocatalytic removal of Malachite green dye from aqueous solutions by nano-composites containing titanium dioxide: A systematic review. Environmental Health Engineering and Management Journal. 2021;8(4):295-302. doi: 10.34172/EHEM.2021.33.
14. Li J, Liu B, Han X, Liu B, Jiang J, Liu S, et al. Direct Z-scheme TiO_2-x/AgI heterojunctions for highly efficient photocatalytic degradation of organic contaminants and inactivation of pathogens. Sep Purif Technol. 2021;261:118306. doi: 10.1016/j.seppur.2021.
15. Orooji N, Takdastan A, Jalilzadeh Yengejeh R, Jorfi S, Davami AH. Photocatalytic degradation of 2, 4-dichlorophenoxyacetic acid using Fe_3O_4@ TiO_2/Cu_2O magnetic nanocomposite stabilized on granular activated carbon from aqueous solution. Res Chem Intermed. 2020;46(5):2833-57. doi: 10.1007/s11164-020-04124-9.
16. Singh S, Kumar V, Anil AG, Kapoor D, Khasnabis S, Shekar S, et al. Adsorption and detoxification of pharmaceutical compounds from wastewater using nanomaterials: A review on mechanism, kinetics, valorization and circular economy. J Environ Manage. 2021;300:113569. doi: 10.1016/j.jenvman.2021.113569.
17. Alibeigi AN, Javid N, Amiri Gharaghani M, Honarmandrad Z, Parsaie F. Synthesis, characteristics, and photocatalytic activity of zinc oxide nanoparticles stabilized on the stone surface for degradation of metronidazole from aqueous solution. Environmental Health Engineering and Management Journal. 2021;8(1):55-63. doi: 10.34172/EHEM.2021.08.
18. Cheng Z, Qi W, Pang CH, Thomas T, Wu T, Liu S, et al. Recent advances in transition metal nitride-based materials for photocatalytic applications. Adv Funct Mater. 2021;31(26):2100553. doi: 10.1002/adfm.202100553.
19. Ahmad N, Alshehri AM, Khan ZR, Ahmad I, Hasan PM, Melaibari AA, et al. Tailoring of band gap, dielectric and antimicrobial properties of silver iodide nanoparticles through Cu doping. Mater Sci Semicond Process. 2022;137:106239. doi: 10.1016/j.mssp.2021.106239.
20. Zhang Y, Lin Z, He Q, Deng Y, Wei F, Xu C, et al. Enhanced aqueous stability and long-acting antibacterial of silver-based MOFs via chitosan-crosslinked for fruit fresh-keeping. Appl Surf Sci. 2022;571:151351. doi: 10.1016/j.apsusc.2021.151351.
21. Alshamsi HA, Beshkar F, Amiri O, Salavati Niasari

M. Porous hollow Ag/Ag2S/Ag3PO4 nanocomposites as highly efficient heterojunction photocatalysts for the removal of antibiotics under simulated sunlight irradiation. Chemosphere. 2021;274:129765. doi: 10.1016/j.chemosphere.2021.129765.
22. Ismail AA, Alsheheri SZ, Albukhari SM, Mahmoud MH. Facile synthesis of visible-light-induced mesoporous Ag2O/Fe2 (MoO4) 3 photocatalysts for degradation of tetracycline. Opt Mater. 2021;121:111505. doi: 10.1016/j.optmat.2021.111505.
23. Amin MM, Jaberian B, Bina B, Sadani M, Hadian R, Bonyadinejad G, et al. Advanced oxidation of the endosulfan and profenofos in aqueous solution using UV/H2O22 process. EnvironmentAsia 2014;7(1):57-64. doi: 10.14456/ea.2014.9.
24. Cui DH, Zheng YF, Song XC. A novel visible-light-driven photocatalyst Ag 2 O/AgI with highly enhanced photocatalytic performances. J Alloys Compd. 2017;701:163-9. doi: 10.1016/j.jallcom.2017.01.106.
25. Zheng Z, Chen C, Bo A, Zavahir FS, Waclawik ER, Zhao J, et al. Visible-light-induced selective photocatalytic oxidation of benzylamine into imine over supported Ag/Agi photocatalysts. Chemistry Europe. 2014;6(5):1210-4. doi: 10.002/cctc.201301030.
26. Amornpitoksuk P, Suwanboon S, Randorn C. Photocatalytic dye decolorization under light-emitting-diode irradiation by silver halides prepared from hydrohalic acids. Mater Res Express. 2019;6(11):115524. doi: 10.1088/2053-1591/ab4a56.
27. Foltyn M, Wasiucionek M, Garbarczyk J, Nowiński J. Effect of nanocrystallization on electrical conductivity of glasses and composites of the AgI–Ag_2O–B_2O_3 system. Solid State Ion. 2005;176(25-28):2137-40. doi: 10.1016/j.ssi.2004.08.049.
28. Li S, Hu S, Xu K, Jiang W, Liu Y, Leng Z, et al. Construction of fiber-shaped silver oxide/tantalum nitride pn heterojunctions as highly efficient visible-light-driven photocatalysts. J Colloid Interface Sci. 2017;504:561-9. doi: 10.1016/j.jcis.2017.06.018.
29. Mkhalid IA, Fierro JL, Mohamed RM, Alshahri AA. Visible light driven photooxidation of imazapyr herbicide over highly efficient mesoporous Ag/Ag2O–TiO2 pn heterojunction photocatalysts. Ceram Int. 2020;46(16):25822-32. doi: 10.1016/j.ceramint.2020.07.064.
30. Ren HT, Yang Q. Fabrication of Ag_2O/TiO_2 with enhanced photocatalytic performances for dye pollutants degradation by a PH-induced method. Appl Surf Sci. 2017;396:530-8. doi: 10.1016/j.apsusc.2016.10.191.
31. Hosseini M, Esrafili A, Farzadkia M, Kermani M, Gholami M. Degradation of ciprofloxacin antibiotic using photo-electrocatalyst process of Ni-doped ZnO deposited by RF sputtering on FTO as an anode electrode from aquatic environments: Synthesis, kinetics, and ecotoxicity study. Microchem J. 2020;154:104663. doi: 10.1016/j.microc.2020.104663.
32. Wang Y, Shen C, Zhang M, Zhang BT, Yu YG. The electrochemical degradation of ciprofloxacin using a SnO2-Sb/Ti anode: Influencing factors, reaction pathways and energy demand. Chem Eng J. 2016;296:79-89. doi: 10.1016/j.cej.2016.03.093.
33. Dien Dang V, Adorna J, Annadurai T, Bui TAN, Tran HL, Lin LY, et al. Indirect Z-scheme nitrogen-doped carbon dot decorated Bi_2MoO_6/g-C_3N_4 photocatalyst for enhanced visible-light-driven degradation of ciprofloxacin. Chem Eng J. 2021;422:130103. doi: 10.1016/j.cej.2021.
34. Le VT, Tran VA, Tran DL, Huong Nguyen TL, Doan VD. Fabrication of Fe_3O_4/CuO@C composite from MOF-based materials as an efficient and magnetically separable photocatalyst for degradation of ciprofloxacin antibiotic. Chemosphere. 2021;270:129417. doi: 10.1016/j.chemosphere.2020.129417.
35. Cuprys A, Pulicharla R, Lecka J, Brar SK, Drogui P, Surampalli RY. Ciprofloxacin-metal complexes–stability and toxicity tests in the presence of humic substances. Chemosphere. 2018;202:549-59. doi: 10.1016/j.chemosphere.2018.03.117.
36. Nekouei S, Nekouei F, Kargarzadeh H. Synthesis of ZnO photocatalyst modified with activated carbon for a perfect degradation of ciprofloxacin and its secondary pollutants. Appl Organomet Chem. 2018;32(3):e4198. doi: 10.1002/aoc.4198.
37. Amin MM, Moazzam A. Use of a UV/H_2O_2 process for posttreatment of a biologically treated composting leachate. Turkish J Eng Env Sci. 2014;38(3):404-10. doi: 10.3906/muh-1409-9.
38. Shah NS, Khan JA, Sayed M, Iqbal J, Khan ZU, Muhammad N, et al. Nano-zerovalent copper as a Fenton-like catalyst for the degradation of ciprofloxacin in aqueous solution. J Water Process Eng. 2020;37:101325. doi: 10.1016/j.jwpe.2020.101325.
39. Abedi M, Ahmadmoazzam M, Jaafarzadeh N. Removal of cationic tolonium chloride dye using Fe3O4 nanoparticles modified with sodium dodecyl sulfate. Chem Biochem Eng Q. 2018;32(2):205-13. doi: 10.15255/CABEQ.2017.1245.
40. Sharma S, Basu S. Highly reusable visible light active hierarchical porous WO_3/SiO_2 monolith in centimeter length scale for enhanced photocatalytic degradation of toxic pollutants. Sep Purif Technol. 2020;231:115916. doi: 10.1016/j.seppur.2019.115916.
41. Arunpandian M, Selvakumar K, Raja A, Rajasekaran P, Thiruppathi M, Nagarajan ER, et al. Fabrication of novel Nd_2O_3/ZnO-GO nanocomposite: An efficient photocatalyst for the degradation of organic pollutants. Colloids Surf A Physicochem Eng Asp. 2019;567:213-27. doi: 10.1016/j.colsurfa.2019.01.058.
42. Makama AB, Salmiaton A, Choong TS, Hamid MR, Abdullah N, Saion E. Influence of parameters and radical scavengers on the visible-light-induced degradation of ciprofloxacin in ZnO/SnS2 nanocomposite suspension: Identification of transformation products. Chemosphere. 2020;253:126689. doi: 10.1016/j.chemosphere.2020.126689.
43. Kordestani B, Takdastan A, Jalilzadeh Yengejeh R, Neisi AK. Photo-Fenton oxidative of pharmaceutical wastewater containing meropenem and ceftriaxone antibiotics: Influential factors, feasibility, and biodegradability studies. Toxin Rev. 2020;39(3):292-302. doi: 10.1080/15569543.2018.1520261.